Wearable Device for Measuring EDA in Constant Alternating Current

David Asiain Ansorena, Jesús Ponce de León Vázquez, and José Ramón Beltrán Blázquez

***Abstract*—This article introduces a novel wearable device, the multisensor wearable wristband (MsW^2), designed to measure electrodermal activity (EDA) and skin temperature using constant ac current instead of the usual constant ac voltage measurement method. Adapted from a previous headband model, MsW^2 has been optimized for wrist-based applications. Its efficacy was validated through experiments with 25 participants, comparing its EDA measurements with the Empatica E4 device. The results demonstrated high coherence between the two systems. Additionally, a simplified skin impedance model was proposed and validated, providing a reliable means of analyzing EDA data. The wearable demonstrates significant potential for applications in emotion detection, health monitoring, and more.**

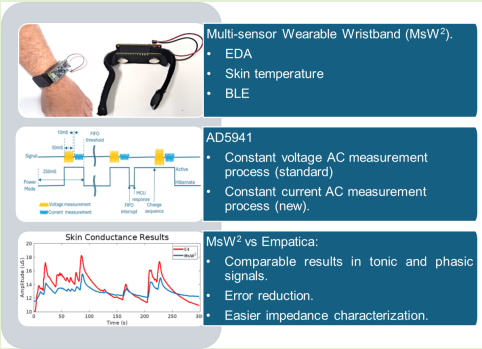

***Index Terms*— AC measurement, EDA measurement, electrodermal activity (EDA), wearable device.**

I. Introduction

ELECTRODERMAL activity (EDA) involves all changes in the electrical properties of the skin (impedance, conductivity, skin potential, and capacitance, among others), mainly due to the activity of the sweat glands [1]. In turn, the sweat glands respond to internal and external stimuli, that is, environmental conditions, different moods, and even the presence of certain diseases or disorders [2]. Thus, EDA can be used both for the direct measurement of the aforementioned electrical parameters of the skin and for the indirect measurement of the activity of the sympathetic system. This activity can be affected by both physical activity and the individual's emotional state, both of which generate different physiological stimuli that alter the activity of the sweat glands [1].

The development of platforms for recording, monitoring, and analyzing EDA signals has grown in recent years [3] and is now a very active branch of sensor electronics. The range of uses of captured EDA signals has expanded proportionally to the diffusion of this technology, from the extraction of health-related characteristics to the classification of emotions or moods. More specific applications of EDA can include diagnosis and monitoring of disease/disorder (autism [4], psychiatric disorder [5], phobia [6], and depression [7], among others), stress detection [8], remote healthcare [9], human–machine interaction [10], rehabilitation processes [11], monitoring of daily activity [12], and general emotion detection [13].

A. Wearable Devices

Wearable devices are intelligent electronic platforms, incorporated into clothing or worn on the body, generally in the form of accessories (forehead bands, bracelets, patches, and watches), which allow the collection of physiological data from the user and, in general, a more or less detailed analysis of these data, with fewer restrictions compared to traditional laboratory devices [14]. Today, the use of wearable devices has become widespread, as well as the signals that these devices are capable of recording and analyzing.

The development of platforms for recording, monitoring, and analyzing physiological signals has continued growing for

Received 20 February 2025; revised 3 March 2025; accepted 4 March 2025. Date of publication 18 March 2025; date of current version 1 May 2025. This work was supported in part by European Union NextGenerationEU/PRTR through the Project Technological Ecosystem for the MOod Recognition in Cardiac Rehabilitation Patients (TEMOR) under Grant TED2021-130374B-C22 and in part by the Aragonese Government under Grant T60_23R. The associate editor coordinating the review of this article and approving it for publication was Dr. Sungyong Jung. *(Corresponding author: David Asiain Ansorena.)*

This work involved human subjects or animals in its research. The authors confirm that all human/animal subject research procedures and protocols are exempt from review board approval.

David Asiain Ansorena and Jesús Ponce de León Vázquez are with the Polytechnic School of La Almunia (EUPLA), University of Zaragoza, 50100 Zaragoza, Spain (e-mail: dasiain@unizar.es; jponce@unizar.es).

José Ramón Beltrán Blázquez is with the School of Engineering and Architecture (EINA) and the Aragon Institute for Engineering Research (I3A), University of Zaragoza, 50018 Zaragoza, Spain (e-mail: jrbelbla@unizar.es).

Digital Object Identifier 10.1109/JSEN.2025.3549513

more than a decade [15] and is now a very active branch of sensor electronics [16]. The range of uses of captured physiological signals has expanded proportionally to the spread of this technology, from the extraction of health-related characteristics to the classification of emotions or moods. More specific applications of physiological signals may include, among others, disease diagnosis [17], remote healthcare [18], [19], human–machine interaction (e.g., to increase the autonomy of people with disabilities) [12], rehabilitation processes [20], stress detection [21], monitoring of daily activity [22], and emotion detection [23].

Last but not least, the algorithms used for feature extraction from physiological signals (and in particular, from EDA) include heuristic algorithms based on traditional techniques such as the wavelet transform [24], algorithms based on neural networks [25], and deep learning systems [26], among others.

B. EDA Measurements

As mentioned in the previous section, EDA is regulated by the sweat glands. In humans, the concentration of these glands is different in different parts of the body [1]. For example, they are especially concentrated on the fingers, palms of the hands, and soles of the feet [27]. Shoulders, feet, and fingers have similar EDA responses [28]. On the other hand, there must be obvious physiological differences between individuals, even depending on the gender of the subject [29]. All this makes the variability in the measurement of EDA extremely high. There are no concrete measures of either the mean level of EDA or the variability of the signal, all of which depend on the individual and his physical and emotional state.

The EDA signal has two main components [1]: the tonic (or electrodermal level, EDL, or longer time courses) and the phasic (or electrodermal response, EDR, the magnitude and number of responses). EDA measurements can be performed without electrical stimulation (endosomatic measurement) [30] or with electrical stimulation (exosomatic measurement) [31]. In the first case, no external voltage source is applied, and the electrodermal potential (measured in mV) is accessed. Endosomatic responses can be monophasic (positive or negative), biphasic, and triphasic [3], so the measurement process and its interpretation can be complicated. However, exosomatic measurements are comparatively easier to obtain and analyze. In exosomatic measurements, a voltage source is connected to the subject, thus obtaining information on the skin resistance (SR) or conductance (SC), if the voltage is dc, or its admittance (SY) or impedance (SZ), if it is ac.

Exosomatic measurements are regulated by the IEC 60 601 standard (UNE-EN 60601-1 [32]), which limits the maximum value of current through the human body for both dc and ac measurements. The application of a dc voltage or current makes it possible to measure the passive electrical properties of the skin (mainly its conductance) [3]. Although this method is the most widespread, it can be subject to errors due to the polarization of the electrodes. This problem is eliminated by the use of constant ac voltages or currents, resulting in a measurement of skin admittance or impedance, respectively. In the ac measurements, the constant voltage measurement is the most commonly used. In this type of measurement, the frequency of the ac signal provides information about the skin at different depths.

The measurement of EDA under constant ac current is much less common [33]. This is probably due to the need for both a constant current value reading and the need to alter the excitation voltage value so that the excitation voltage measurement does not vary excessively, which complicates the system at both the hardware and software levels. However, this method can have great advantages inherent in the use of constant current, such as being less important for the nature of the electrodes, which will be discussed next.

Indeed, the selection of appropriate electrodes is often one of the most important issues in EDA measurement. On the one hand, there are gel electrodes, in which a substance (liquid or solid) is placed that facilitates electrical contact between the skin and the electrode, increasing the quality of the signal [34]. The electrical properties of the gel and its degradation are vital in these cases [3]. These types of electrodes are usually more sensitive to electrical noise. However, dry electrodes, without electrolytes to facilitate ionic transport between the skin and the electrode surface, generate more capacitive charge transfer and therefore a greater dependence on the excitation frequency measurement. Lacking the adhesion of the gel, these electrodes do not provide a stable contact with the skin and the measurements can present large discontinuities, even with small variations in the contact pressure between the electrode and the skin. On the other hand, they do not degrade over time and provide more stable long-term readings [34].

C. AD5941 Bioimpedance Shield

The AD5941[1] is a state-of-the-art, low-cost, high-performance sensor, including a wide operating frequency range, high-resolution analog-to-digital conversion, and the ability to perform two-to-four terminal impedance measurements. It has a transimpedance amplifier with a variety of feedback resistors to measure a wide range of electrical impedances. The AD-5941 uses two different power supplies: 1.8 V for the digital part and 3.3 V for the analog part.

The AD5941 Bioimpedance shield is presented as a cost-effective, high-performance solution for a variety of applications. In [35], it is used to build a portable and low-cost electrochemical impedance spectroscopy system for lithium-ion batteries. A low-cost portable impedance analyzer designed for bioimpedance applications, in a biomedical context and specifically for sarcopenia detection and electrochemical quantification, is described in [36]. In [37], the AD5941 is integrated into a compact impedance measurement system for the detection of A549 lung cancer cells. Finally, in [38], the AD5941 is used to develop a high-precision, low-cost, and easy-to-use device that measures in situ the electrical conductivity of soil, for agriculture and forestry applications.

In this work, an EDA signal measurement device based on the AFE-AD5941 is presented. It is developed for portable and wearable devices and has high accuracy and low power

[1] https://www.analog.com/en/products/ad5941.html.

consumption. The details of the development of this EDA measurement system will be detailed later.

D. Organization of This Article

As mentioned above, this article will detail the development of a wearable platform for the capture of biomedical signals. In Section II, a simplified model for the skin is proposed that allows us to obtain a new variable on which it would be feasible to perform EDA activity measurements. Sections III and IV describe from different points of view the hardware of the device responsible for the acquisition, saving, sending, and/or processing of data of the different biomedical magnitudes to be measured, paying special attention to the EDA activity, which is the main focus of our work. Section V summarizes the most important aspects of the software program in the device, paying special attention to the constant ac current measurement process in comparison with the standard technique. In Section VI, the main results of the device measurements are shown. Finally, Section VII presents the conclusions of the work.

II. Skin Impedance Model

The general variation in skin impedance is mainly related to the activity of the sweat glands. The capacitance variation in these glands is also induced by sweat since sweat acts as the dielectric of a capacitor in these glands. The capacitance and resistance values of the epidermis and the resistance values of the dermis are different for each user but show a low fluctuation. Depending on the depth at which the tissues are analyzed and the required accuracy of the results, the skin impedance model can be quite complex and involves, in general, and without going into detail, several resistors and capacitors interconnected in a complicated network of series and parallels [1], [39]. The electrode electrical model itself involves a resistor in parallel with a capacitor, with a voltage source in series to these.

In our case, we have opted for a much simpler skin impedance model, consisting of a single resistor in parallel with a single capacitor. Since in the measurement process to be detailed later, both voltages and currents will be complex numbers, it is possible to have access to the real and imaginary part of the skin impedance, which allows us to obtain separately, as will be explained below, the resistive and capacitive part of the model.

The multisensor wearable wristband (MsW^2) device, as mentioned above, performs an ac impedance measurement. This allows us to reconstruct the signals corresponding to the skin resistance and capacitance of each individual, using only the real (X) and imaginary (Y) parts recovered from the impedance data recorded by the device.

Starting from the definition of the complex impedance of resistor and capacitor in parallel, it can be seen that the real and imaginary parts are

$$X = \frac{R}{1 + R^2\omega^2C^2} \tag{1}$$

and

$$Y = \frac{R^2\omega C}{1 + R^2\omega^2C^2}. \tag{2}$$

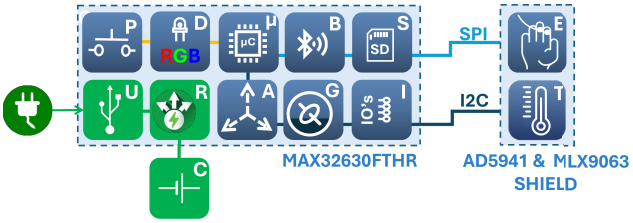

Fig. 1. Block diagram of the prototype.

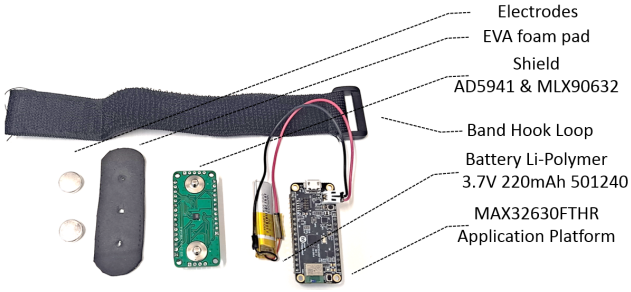

Fig. 2. Real image of the MsW^2 prototype.

From where the values of skin resistance (R) and skin capacitance (C) can be deduced

$$R = X\left(1 + \frac{Y^2}{X^2}\right) \tag{3}$$

$$C = \frac{-Y}{\omega\left(X^2 + Y^2\right)}. \tag{4}$$

This model has been applied in this work to obtain the resistance and capacitance data presented in Section VI-D. In advance of these results, both the information extracted from the resistive (conductive) part of the skin and its capacitive part allows EDA analyses to be performed with potentially equivalent results.

III. Prototype Description

This section describes the prototype design and the most significant components included. In addition, interesting features and the relationship between components are detailed. The block diagram of the prototype is shown in Fig. 1.

As can be seen in Fig. 1, the prototype wearable EDA measurement device presented here is based on the MAX32630 FTHR kit (Maxim Integrated) and a self-developed bioimpedance shield. These two components offer the versatility of a wearable platform for EDA and bioimpedance measurement, with a lightweight, comfortable, wireless, removable, and expandable sensor with battery autonomy for research developments.

The prototype is shown in Fig. 2 and incorporates a small lithium polymer battery with a 3.7-V cell. Charging/discharging of the battery is managed by a battery charge manager, which has a smart power selector to reduce battery consumption. The board development kit contains the microcontroller, an accelerometer/gyroscope, a battery charge manager, a battery connector, a dual-mode Bluetooth low-energy module, a micro-SD card connector, as well as an

input/output interface consisting of a push button and an RGB led to indicate the actual device or measurement status.

The size of the board is compact, 0.9 × 2 in, and the BioImpedance shield is based on this size to fit perfectly. In addition, the BioImpedance shield features an EDA sensor, a temperature sensor, and expansion ports to allow expanding the capabilities of the platform, both of which work with lower power consumption and are based on the latest technology. The main components of the MAX32630 FTHR and Bioimpedance Shield are described next.

IV. Hardware Description

A. MAX32630 FTHR Kit

As advanced in the previous section, the developed prototype incorporates a small lithium 3.7-V battery whose charge/discharge is controlled by the MAX14690[2] battery charge management circuit, an ideal solution for low-power wearable devices. This kit also contains the microcontroller, MAX32630,[3] a high-efficiency microcontroller for wearable devices, and the BMI160,[4] a low-power inertial meter capable of measuring acceleration and angular velocity. The use of gyroscopes/accelerometers is important in wearable devices because, in addition to sending information about the user's position and movements, it allows to correct (through a simple correlation) the artifacts caused by physical activity in other monitored variables, as in our case, the EDA signal. Finally, the MAX32630 FTHR kit contains the PAN 1326B,[5] a Bluetooth low-energy (BLE version 4) module and other connectors and indicators cited before.

B. EDA Module

The developed shield incorporates an integrated circuit for the acquisition of the EDA signal, the AFE-AD5941. It is developed for portable and wearable devices and has high accuracy and low power consumption. The device is capable of generating a voltage signal with up to 12-bit resolution and 200-kHz frequency. The device has two measurement loops: the low-bandwidth loop with an operation frequency of up to 200 Hz and the high-bandwidth loop with a frequency range from 200 Hz up to 200 kHz.

It has a transimpedance amplifier with a variety of feedback resistors to measure a wide range of skin current values. The AD-5941 uses two different power supplies: 1.8 V for the digital part and 3.3 V for the analog part. In addition, it incorporates a DFT hardware block and a digital filter to process the signal, so it can work with ac signals and obtain the complex parameter of skin impedance (real and imaginary parts), facilitating, among other things, the use of different types of electrodes, such as dry electrodes. The device is independent of the microcontroller as it has its sequencer which can store a measurement configuration, providing signal generation and skin impedance measurement. Communication with the microcontroller is done only to send the measurement data and to notify the need for reconfiguration (e.g., to change the amplitude of the generated signal).

C. Electrode Configuration

The shield has the great advantage of directly connecting two electrodes to perform the skin conductivity measurement. In addition, this shield can be used in other different configurations to measure skin impedance, such as 3- or 4-wire measurements. Two output loops are available, each one with a decoupling capacitor and a limiting resistor, with the idea that both comply with the current standard, IEC60601, and the current flowing through the skin tissue is less than 10 μA, thus avoiding any damage. The operation of both measurement modes is explained in Section V-B. The device also has a set of pins for connecting different types of electrodes.

D. Skin Temperature

Finally, the developed shield incorporates the MLX90632,[6] a small noncontact infrared temperature MLX90632 with 50° field of view (FoV). The manufacturer has previously calibrated this device to achieve high accuracy by storing its configuration in an EEPROM memory. Its specific encapsulation reduces thermal disturbances. The sensor has the necessary electronics to digitize and filter the temperature information, which is stored in RAM to be sent to the microcontroller. In addition, the MLX90632 can measure its own temperature. The sensor power supply is 3.3 V, with an active current of 1 mA (quiescent current less than 2.5 μA). The temperature sensor uses the I2C protocol, which in our prototype operates at 1.8 V. This device has different presentations, standards, and medical, whose most significant difference is in its accuracy. The medical version is factory calibrated with an accuracy of ±0.2 °C and has a resolution of 0.01 °C. In addition, it has three operating modes: idle mode, step mode, and continuous mode. The difference between the latter two is the measurement frequency: the step mode performs a measurement only when requested by the microcontroller.

V. SC Measurement

To obtain skin conductance (SC), our prototype uses the previously presented device AFE-AD5941, as a signal generator and data acquisition system. This powerful chip has all the necessary components to measure the analog signal and perform the digital signal processing.

A. Integrated Circuit Description

All components involved in the SC measurement process can be seen in Fig. 3. At the top of the figure, block (1), the sinusoidal waveform generator is shown. It can be seen that the low-power DAC (LPDAC) has two outputs, one of them (12 bits) fed from the waveform generator and another (6 bits) configured to add the offset of the current signal in the current-to-voltage conversion stage, denoted as block

[2]https://www.analog.com/en/products/max14690.html.
[3]https://www.analog.com/en/products/max32630.html.
[4]https://www.bosch-sensortec.com/products/motion-sensors/imus/bmi160/
[5]https://na.industrial.panasonic.com/products/wireless-connectivity/bluetooth/lineup/bluetooth-multi-mode/series/90894.
[6]https://www.melexis.com/en/documents/documentation/datasheets/datasheet-mlx90632

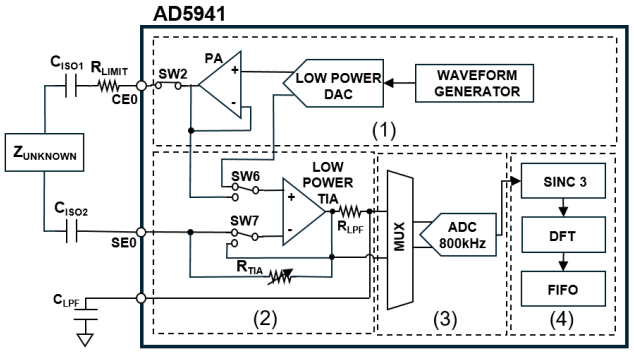

Fig. 3. SC measurement block diagram. (1) Sine waveform generator. (2) Transimpedance (LPTIA) amplifier. (3) LPTIA feedback resistance multiplexer and ADC. (4) DSP module. Inspired and redrawn from [?]db@bib:35.

(2) in Fig. 3. The amplitude and frequency of the signal are set with the waveform generator. The output voltage range is 0.2–2.4V and the sampling frequency in our application is 100 Hz.

The LPDAC analog signal appears at the CE0 output through a low-noise potentiostatic amplifier whose output is configured as a standard buffer. This signal reaches the skin through the capacitor C_{ISO1}, which eliminates the signal bias, as well as any dc current from the human skin and electrodes (Z_{unknown}). The voltage signal at the SE0 pin is coupled to the bias voltage through C_{ISO2}, which is the input to the low-power transimpedance amplifier (LPTIA). We will return to this point later.

The LPTIA performs a current-to-voltage conversion, using a resistance (R_{TIA}) with a capacitor in parallel (C_{TIA}, not shown in Fig. 3 for simplicity) in the negative feedback loop. The resistance used is one of a set of 25 programmable resistances which can vary from 200 Ω to 512 kΩ. This allows amplifying the current signal and obtaining a better digital-to-analog conversion by being able to use the whole input voltage range. The converted voltage signal is then lowpass filtered through R_{LPF} and C_{LPF}.

To obtain the digital signal needed, block (3) in Fig. 3, the integrated circuit uses a multiplexer that selects the input to the 16-bit ADC. This ADC (which operates at a sampling rate of 800 k samples per second) has a differential input. The signals employed are, on the one hand, the voltage filtered in the previous stage, and, on the other hand, the negative input of the low-power transimpedance amplifier (LPTIA_N).

Finally, the digital signal-processing module, block (4) in Fig. 3, has different stages. In the first one, after the digitization process, the signal is reduced by a factor of 3 (SINC3) without loss of information. Then, a digital Fourier transform (DFT) is processed through a block that performs a frequency sweep on the data and generates an output with real and imaginary parts (of 18-bit resolution) only for the frequency set in the waveform generator, thus eliminating any other remaining frequency information. The DFT is stored in the FIFO. The microcontroller is notified when the FIFO is full.

B. SC Measurement Methods

The chip's developer, Analog Devices, proposes a proprietary SC measurement method based on a constant ac voltage. An alternative method, based on a constant ac current, has been designed for the developed device. The use of dc or ac signals gives different impedance (conductance) results as the frequency of the signal passes through the skin at different depths [3]. A common point of both methods may be the excitation frequency, which must be below 120 Hz to measure EDA. As will be seen below, in the comparison of results both methods work with an excitation signal at 100 Hz.

Both methods will be explained next.

1) Constant DC Voltage (Analog Devices): The method proposed by Analog Devices consists of maintaining the chip's internal generator voltage, marked as (1) in Fig. 3, at its maximum value (1.1 V) by measuring the SC (impedance) through a variable gain (controlled mainly through R_{TIA}) in the LPTIA amplifier, block (2) in Fig. 3. As mentioned above, by regulation the current flowing through a human being must be 10μA maximum (IEC60601). This value is ensured by calculating a limiting resistor (R_{LIMIT}) and coupling capacitors (C_{ISO1} and C_{ISO2}) in the measurement network, that also includes the unknown skin impedance (see again Fig. 3). Calculating so that [40], even under short-circuit conditions, the current flowing through this branch does not exceed the above limit, we have that $R_{\mathrm{LIMIT}} = 1$ kΩ, $C_{\mathrm{ISO1}} = 15$ nF, and $C_{\mathrm{ISO2}} = 470$ nF.

Using this impedance network and knowing the voltage (1.1 V) and current (measured) values between the CEO and SEO pins of the device (Fig. 3), the value of the skin impedance (conductance), Z_{unknown}, can be obtained.

As the measured SC changes, the device adapts the impedance of the LPTIA feedback loop to obtain the optimum amplification in the current measurement process. An undesirable result of this is that each time the R_{TIA} resistance changes, discontinuities occur in the measurement of SC that, if uncorrected, can be mistaken for events in the phasic signal being extracted from the EDA. However, this drawback can be overcome since R_{TIA} value is stored in the device measurements. By analyzing the value of this resistance at each time stamp, these jumps can be detected and corrected easily. However, the procedure is cumbersome and, if not processed properly, may leave spurious remainders in the signal that could lead to false EDA activity positives.

2) Constant AC Current: Holding constant a current over an unknown and variable impedance is not possible. However, what can be achieved is to maintain a current that remains *approximately* constant during the process of measuring the unknown impedance. The procedure itself is not conceptually complicated. Through the measurement of voltage and current, in the same way as in the procedure described above, the value of the skin impedance Z_{unknown} can be obtained. Using the last calculated impedance value, the voltage value required to keep the current fixed in the next measurement is easy to obtain using the same equation. This is basically the procedure that has been developed, which will be explained in detail in the following paragraphs.

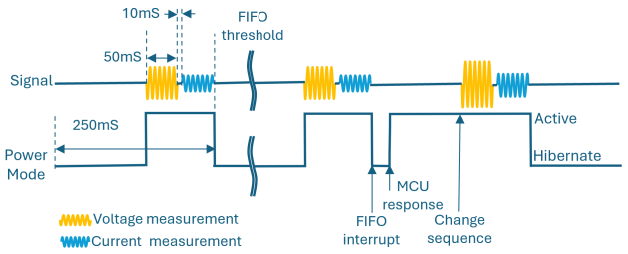

Fig. 4. Constant current source measurement sequence (see text for details).

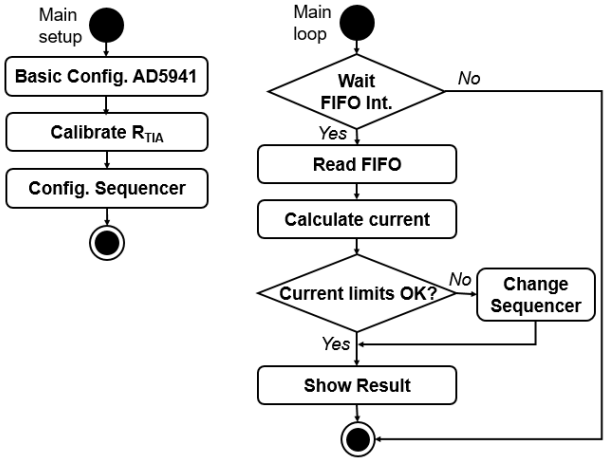

Fig. 5. Microcontroller UML diagram for EDA measurement.

By altering the component values obtained for the procedure proposed by Analog Devices (between the CEO pins and SEO pins of the AD5941), the proposed system incorporates a loop in which the current control is performed by software. In this case, C_{ISO1} and C_{ISO2} are worth 1 μF and $R_{\mathrm{LIMIT}} = 1$ kΩ. In this way, the device is potentially capable of sending higher currents.

The prototype uses a constant current source that modifies the voltage amplitude to inject an invariant current (the maximum possible current, always limited to the standard IEC60601) into the skin, adapting to the impedance value. This method has a number of advantages which will be detailed later.

The measurement sequence is shown in Fig. 4. This sequence differs from the measurement sequence proposed by Analog Devices explained before, due to the quasisimultaneous measurement of voltage and current, which allows measuring voltage and current without having to configure the microcontroller.

In the first step, the amplitude of the voltage signal is set to a low value, to limit the initial current. At that time (yellow signal in Fig. 4), the chip is set to measure the voltage. This signal is triggered for 50 ms, and after a 10 ms wait to stabilize the signal, the microcontroller is configured to measure the current, using the same excitation signal, which is generated for another 50 ms (in blue in Fig. 4). This process is repeated every 250 ms. The signals from the measurement process are converted from analog to digital, processed, and stored in the FIFO. Each measurement generates eight sets of data, four sets of real and imaginary parts of current and voltage. Thus, when the FIFO has exactly 16 data, the microcontroller is notified, and the information is sent to calculate a single conductance value.

After the first impedance measurements, this impedance value is used to calculate how much the excitation voltage should be worth in the next cycle to provide a maximum current on the skin, never exceeding the 10-μA limit but staying as close to it as possible. This is not always achievable, of course. Since the maximum excitation voltage of AD5941 is 1.1 V, the maximum value limited by the regulation (10 μA) is only possible for skin impedances below 110 kΩ (or about 9 μS of conductance). If the skin impedance is higher than 110 kΩ, the algorithm will inject the maximum possible current, reserving a small margin to adapt this value to variations in the EDA signal. In the following cycles, the impedance value is used to calculate how much the excitation voltage must be worth so that the current through the skin remains constant.

During each of these measurement phases (lasting 110 ms), the chip is set to active mode and operates with a low-frequency clock to optimize power consumption. Since four measurements per second of impedance are taken, the rest of the time (140 ms) the chip remains in hibernation mode and uses a high-frequency clock to perform SPI communication. In this way, when the device alerts the microcontroller to take data, the configuration is set immediately, without any delay in the measurement sequence.

The microcontroller and the AD5941 need to be in permanent contact to correctly perform the measurement process. Fig. 5 shows the unified modeling language (UML) diagram of the microcontroller. As can be seen in the figure, the microcontroller executes a basic configuration of the AD5941 which specifies the FIFO working mode, data limit, set voltage reference, and so on. The calibration of R_{TIA} requires a special configuration, in which a calibration can be performed to the whole set of 25 resistances or just to one of them. Once the measurement process explained in the previous paragraphs has been launched, the microcontroller verifies the FIFO stage and, as long as it is not full, it launches the next voltage and current measurements. If the measured current differs from 10 μA, the AD5941 sequence is reconfigured so that the amplitude of the voltage signal keeps the current constant and as high as possible in the next measurement.

Fig. 6 shows in detail the voltage/current measurement sequence in the AD5941. As explained above, this sequence generates a sinusoidal signal and measures voltage and current consecutively, with only a few milliseconds delay. As can be seen in the figure, the voltage measurement process requires the use of the DAC, the LPTIA is configured to measure the voltage, the signal is converted to digital, and the data is processed with the digital filter and the DFT. The result is stored directly in the FIFO. After 10 ms of waiting, another signal is generated independent of the previous one, with conditions as similar as possible to this one and avoiding the phase difference in the DFT calculation. In this case, the LPTIA

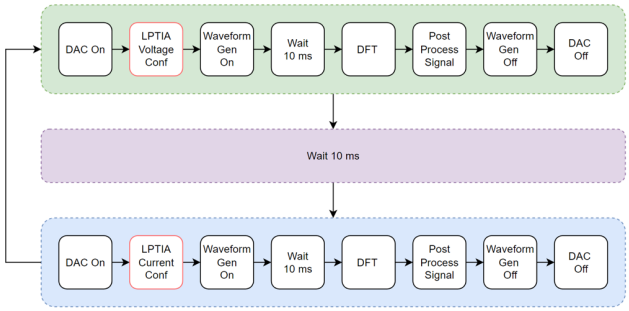

Fig. 6. Sequence of voltage/current measurement.

is configured to perform a voltage-to-current conversion. The voltage thus generated is applied to the skin, through which circulates a current related to the conductance of the skin, which will be obtained through the data obtained, stored in the FIFO.

3) Qualitative Comparison: The interesting thing about the new proposed method of impedance (conductance) measurement is that the injected current will be approximately constant throughout the measurement process, with the advantages inherent in any current measurement process, such as greater noise immunity.

As explained above, to perform precision measurements, the constant voltage method selects the optimal feedback resistance (R_{TIA}) as the skin impedance changes, leading to discontinuities in the EDA signal that must be corrected to avoid false activity markers in the phasic signal. The constant current measurement process can work perfectly well using a single feedback R_{TIA}, which has several important advantages. Most obviously, discontinuities in the EDA signal due to the change in the LPTIA feedback loop are avoided. An additional advantage is that, if a correction in the measurements due to the thermal drift of the device becomes necessary, it is much simpler to work with a single resistor than to work with a total set of 25 resistors.

A quantitative analysis of the comparative results of these methods is shown in Section VI-C.

C. EDA Measurement

Finally, to test the ability of the MsW^2 device to record EDA signals, an experiment was conducted in which a set of individuals were subjected to visual stimuli (by viewing video segments extracted from movies and documentaries), including the emotions fear, anger, joy, disgust, sadness, and boredom. The room in which the test was conducted is isolated from other stimuli. Each participant is fit with a series of sensors to capture different biometric signals such as EEG (through a Muse[7] placed on the forehead), facial expression (with a bull's eye camera placed on a fixed mount), and EDA, captured with two devices: the Empatica (E4) wristband and the MsW^2 platform. The electrodes for measuring the EDA signal are placed on the fingers of the nondominant hand (to reduce as much as possible the noise caused by movement), reserving the index and middle fingers for E4 and the ring and little fingers for MsW^2.

The total duration of the experiment is about 40 min, during which videos with different emotional content will be shown, separated by a neutral video. The corresponding EDA signals thus obtained have been cut into 5-min segments. All signals in which one of the devices exhibited any kind of misbehavior (loss of connection, spurious reflex movement, general electrical noise, etc.) were discarded.

The total number of individuals, of both sexes and between 22 and 50 years old (mostly student volunteers), was 25. The previous selection of signals, based on the criteria set out above, has left us with a total of 43 valid cuts of 5 min each.

Some results of this experience will be shown in the next section, to demonstrate that both the developed platform and the proposed measurement algorithm are perfectly valid for the capture and analysis of the EDA signal.

VI. Results

The developed device has undergone a battery of tests to prove its effectiveness. The results of such tests will be shown in the following sections. First, the battery consumption of the device will be discussed, followed by the response speed of the temperature sensor that measures the skin temperature and whose information could be used to perform a thermal drift correction in the measurement process. Next, we will show the analysis of the differences in impedance measurement using the methods explained in Section V-B, namely at constant ac voltage and constant ac current. The results obtained in obtaining the skin resistance and capacitance introduced in the proposed model (Section II) will be shown later. Finally, EDA signals obtained in the small test explained in Section V-C will be presented.

A. Power Consumption

The power consumption of the entire device was measured in both data capture and Bluetooth transmission modes. The average power consumption obtained under these conditions is 10 mA rms, so the battery autonomy reaches 22 h. On the other hand, thanks to the MAX14690 battery manager, the standby consumption is only 600 nA. Therefore, in this case, the self-discharge factor of the battery is more important than the consumption of the device itself, so the estimated battery life would be more than one year.

B. Temperature Time Response

Regarding skin temperature measurement, as mentioned above, the MsW^2 prototype has an MLX90632SLD. This integrated one has a resolution of 0.01 °C and an accuracy of ±0.2 °C, while the E4 device has a resolution of 0.02 °C and ±0.2 °C. The response times of both measuring devices have been compared. The result is a response time of 1.9 s for the E4 versus 3.1 s for the MsW^2 device. Therefore, both sensors, based on IR technology, have a short response time compared to other technologies [40].

[7]https://choosemuse.com/

TABLE I
PERFORMANCE RESULTS. CACV: CONSTANT AC VOLTAGE METHOD (ANALOG DEVICES). CACC: CONSTANT AC CURRENT METHOD (PROPOSED)

Z_{real} (kΩ)	CACV Error (%)	CACC Error (%)
50	1.47	0.13
100	1.02	0.11
270	0.33	0.11
560	0.035	0.2
1000	0.082	0.023

C. Performance Results

To compare the proposed new measurement sequence, at constant current, with the one proposed by Analog Devices, a test is performed by taking a set of samples at different standard resistors (50, 100, 270, 560 kΩ, and 1 MΩ). These resistors were measured with a calibrated high-performance multimeter (FLUKE, model 43). Only the real part of each impedance is analyzed since the parasitic capacitor is difficult to obtain. The results are shown in Table I, indicating the real part of the impedance in kΩ.

In the results shown in Table I [41], a clear reduction of the relative error can be observed in the measurement of electrical resistance in this set of standard resistors with respect to the constant voltage measurement method. In fact, the error remains below 0.2%, even for low resistance values, so the use of this novel sequence allows a more accurate impedance measurement system.

These results are very close to the technological limitation of the Electrodermal Front End AD5941. For example, in [42], where an AD5941 is used for a totally different application, the results in the accuracy of the resistive part of the impedance to be measured, always below 0.5%, are very similar to those shown here.

D. Skin Impedance Model Results

As anticipated in Section II, a simplified impedance model for the skin has been applied. In that model, the measured impedance consists of a resistor in parallel with a capacitor. From the EDA signals captured during the experiment detailed in Section V-C, by applying relevant equations (see Section II), the activity corresponding to the SC and capacitance can be separated.

This allows us to retrieve the values of both skin resistance and capacitance from our simplified model from the ac signals collected by our measurement system. In Fig. 7, the instantaneous skin resistance, conductance, and capacitance values extracted from the model are presented. Observe how the variations of all signals (specifically conductance and capacitance) appear highly correlated. As will be shown later, tonic and phasic signals, which are crucial in EDA analysis, are extracted from this information. This means that skin capacitance could also be used to detect EDA activity with potentially as accurate results as those achieved through SC.

The validity of the proposed skin model can be seen in Fig. 8, where the direct SC result obtained by the Empatica wristband for a given individual is compared with the result obtained by MsW^2 for the same individual in the same time

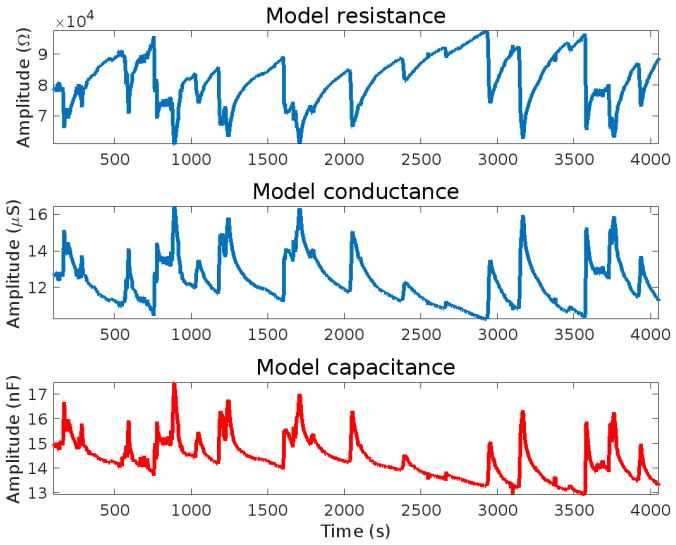

Fig. 7. Skin resistance and conductance (blue) and capacitance (red) extracted from the proposed simple model.

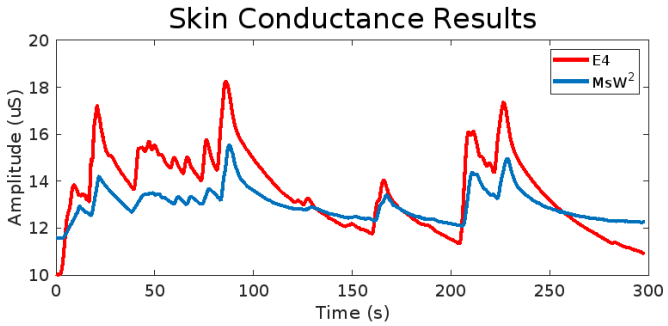

Fig. 8. SC extracted from E4 data (in red) and the proposed skin mode and MsW^2 data (in blue). Both results are in μS.

frame, after applying this model. The differences between the two signals may be because the EDA measurements were taken for both devices between different fingers of the participant's hand, always respecting the same order of the sensors.

The application of this impedance model to the skin provides an important advantage for the subsequent analysis of the signal. Both the results are shown in Fig. 8 and those to be shown in Section VI-E are the signals directly obtained through the model presented here. When this model is not applied, as is the case, for example, in [43] (in which a comparison is made between a device built with an AD5940, similar to the AD5941 used here, and a commercial BioSignalPlux[8] device), a renormalization of the EDA signal is generally necessary before proceeding to its analysis. This normalization affects the skin impedance values but not its overall shape. Therefore, from this normalized signal, the tonic and phasic signals are obtained by the usual method, which will be detailed later.

E. Analysis Results

The conductance signals obtained from the raw data captured by both measurement systems are smoothed using a

[8]https://www.biosignalsplux.com/index.php/researcher.

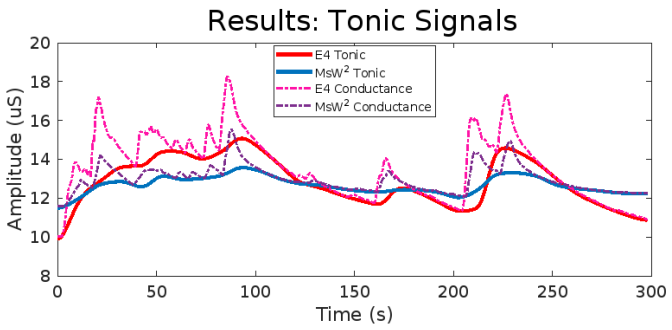

Fig. 9. Tonic signals. In blue, the MsW^2 tonic signal, obtained from the MsW^2 conductance (red dotted line). In red, the Empatica tonic signal obtained from the Empatica conductance (blue dotted line). Both results are in μS.

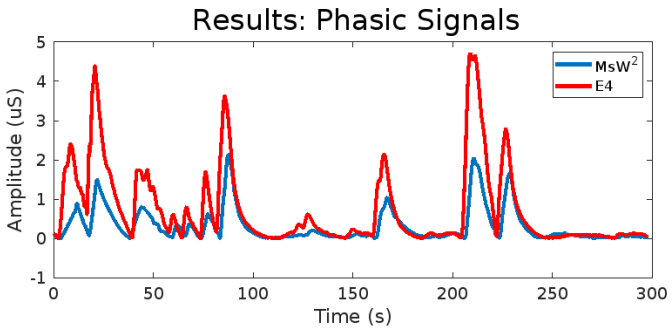

Fig. 10. Phasic signals obtained from the MsW^2 data (blue) and Empatica (red). Both results are in μS.

zero-phase digital filter and analyzed using LedaLab.[9] Ledalab is an open-source code MATLAB tool that automatically obtains both the tonic and the phasic part of the EDA signal under analysis, obtaining for each of these their corresponding excitation signals (or driver). These driver signals, in turn, indicate the time instants in which sufficiently intense changes occur in the signal (tonic or phasic). The tonic signal can be understood as a kind of basic (low-frequency) level that marks the general state of the individual's EDA response. The phasic signal obeys the emotional response to the stimulus, resulting in a series of peaks that vary more rapidly over time and generally decrease over time until the next stimulus arrives.

An example of the extraction of the tonic signal can be seen in Fig. 9. In the figure, the dashed lines show the conductance obtained through E4 (red) and the MsW^2 platform (blue). The tonic signal obtained from the MsW^2 data is shown in blue, while the tonic signal extracted from the Empatica wristband is shown in red.

An example of the phasic signal obtained by Empatica and MsW^2 can be seen in Fig. 10. The phasic signal is the difference between the measured conductance and the tonic signal extracted in each case for the Empatica (red) and the MsW^2 (blue) shown in Fig. 9.

These signals are the responses to the different stimuli to which the individual under study is subjected, so there is an obvious relationship between the most immediate emotional response and the phasic signal obtained by this procedure.

[9]Available in http://www.ledalab.de/software.htm.

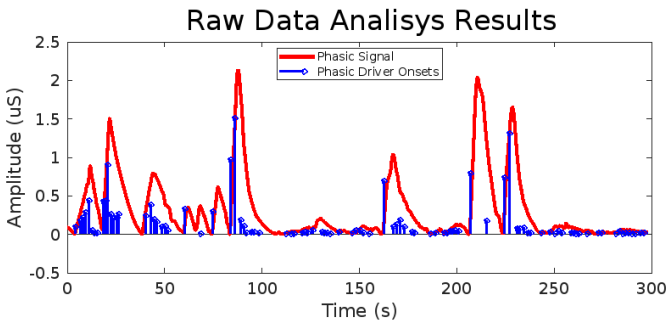

Fig. 11. Continuous line: phasic signal from the MsW^2 data. The onsets of the phasic driver signal are shown as blue vertical lines.

TABLE II
PERCENTAGE OF COINCIDENCES BETWEEN E4 AND MSW^2 EDA SIGNALS. HMS: HANDMADE SELECTED PEAKS (SEE TEXT)

% Peaks (Approx.)	Ground E4	Ground MsW^2
100	92.3255	93.8934
75	81.1383	81.5259
50	75.7551	76.2749
25	67.9287	68.7704
0	61.3212	60.8101
HMS	94.9336	94.8468

In other words, by analyzing the phasic signal, the emotional response of the subject to the different stimuli can be derived. This objective is beyond the results shown in this work, where the main objective is to demonstrate that the EDA information obtained using the E4 wristband and the MsW^2 platform is equivalent.

1) Percentage of Similarity: As explained above, each 5-min signal analyzed corresponds to the emotional response of the same individual to each stimulus in that period of time, captured through two different devices. To validate the results obtained, we will compare the results for each of these two signals, analyzing the onsets calculated from the corresponding drivers of their phasic signals, to verify the possible relationship between the different (but equivalent) onsets. An example of a phasic signal and its corresponding driver onset is shown in Fig. 11.

The onsets in the phasic show the time instants in which changes in the signal have occurred. The number of events selected for further analysis can be controlled by simple filtering. This filtering basically consists of varying an amplitude threshold. The events whose amplitude exceeds this threshold will be considered valid onsets, while the rest will be rejected.

Table II shows the results of the percentage of success in the onsets obtained in the EDA signals through the E4 and MsW^2 for different degrees of peak filtering. The first data correspond to 100% of the peaks detected for both signals. In the first column, the total number of onsets detected by Empatica, and in the second column, the onsets detected by MsW^2 are taken as a basis. The percentage of coincidence is obtained through the number of coincident onsets. Two onsets (one from Empatica, and the other from MsW^2) are considered coincident if they are separated by a maximum of two time stamps. In later rows of the table, an increasing degree of filtering has been applied at the onset level, until the initial

number of peaks is reduced to (approximately) 75%, 50%, and 25% of the initial detected events. The fifth row leaves only the essential event marks for each signal (generally between 5 and 10). In the last row, a human operator has manually selected (HMS in Table II), and the onsets related to the most marked emotional variations in both signals. The final data in the table show the percentages of similarity found in this way.

As can be deduced from the results, there is a great similarity between the onsets marked in the signals obtained in both devices.

VII. Conclusion

The MsW^2 has been successfully developed as a novel wearable device for measuring electrodermal activity (EDA) and skin temperature. It is designed for wrist-worn applications and uses an alternative method of impedance (conductance) measurement to improve signal quality. This alternative method, based on a constant alternating current, was designed for the AFE-AD5941 device to measure SC. The prototype uses a constant current source that modifies the voltage amplitude to inject an unchanging current into the skin, adapted to the impedance value. The constant current measurement method shows a reduction in relative error compared to the constant ac voltage method proposed by Analog Devices, as demonstrated by tests with standard resistors.

The MsW^2 demonstrates high consistency with the Empatica E4 device in EDA measurement, as validated by experimental results with 25 participants. Analysis of the EDA signals obtained with the MsW^2 and the Empatica E4, using visual stimuli to induce different emotions, showed a high similarity between the signals and the detected onsets. This indicates that the MsW^2 can obtain EDA signals with an accuracy comparable to that of the Empatica E4.

A simplified skin impedance model was proposed and validated that allows analysis of EDA data by extracting both skin resistance and capacitance, enabling accurate detection of EDA activity. As has been seen, the variation in skin capacitance is susceptible to be used to extract the same information obtained through conductance, given the high correlation between both variables.

MsW^2 presents potential applications in emotion detection and health monitoring, offering advantages such as the ease of characterizing the total loop impedance and the absence of discontinuities associated with scale change.

In future work, the use of a constant current-based measurement decreases the dependence on electrode properties of different technologies allowing more affordable developments for the design of commercial wearable devices. In addition, the flexibility of the device allows for skin impedance measurements at different frequencies, developing a more complete model of skin impedance.

Acknowledgment

The authors acknowledge Cristian Chacha for his participation in developing the initial work necessary to prepare this work.

References

[1] W. Boucsein, *Electrodermal Activity*. Cham, Switzerland: Springer, 2012.

[2] M. Sharma, S. Kacker, and M. Sharma, "A brief introduction and review on galvanic skin response," *Int. J. Med. Res. Professionals*, vol. 2, no. 6, pp. 13–17, Dec. 2016.

[3] C. Tronstad, M. Amini, D. R. Bach, and Ø. G. Martinsen, "Current trends and opportunities in the methodology of electrodermal activity measurement," *Physiological Meas.*, vol. 43, no. 2, Feb. 2022, Art. no. 02TR01.

[4] M. Taj-Eldin, C. Ryan, B. O'Flynn, and P. Galvin, "A review of wearable solutions for physiological and emotional monitoring for use by people with autism spectrum disorder and their caregivers," *Sensors*, vol. 18, no. 12, p. 4271, Dec. 2018.

[5] U. Desai and A. D. Shetty, "Electrodermal activity (EDA) for treatment of neurological and psychiatric disorder patients: A review," in *Proc. 7th Int. Conf. Adv. Comput. Commun. Syst. (ICACCS)*, vol. 1, Mar. 2021, pp. 1424–1430.

[6] J. Wendt, M. Lotze, A. I. Weike, N. Hosten, and A. O. Hamm, "Brain activation and defensive response mobilization during sustained exposure to phobia-related and other affective pictures in spider phobia," *Psychophysiology*, vol. 45, no. 2, pp. 205–215, Mar. 2008.

[7] J. Kim, B. Ku, J.-H. Bae, G.-C. Han, and J. U. Kim, "Contrast in the circadian behaviors of an electrodermal activity and bioimpedance spectroscopy," *Chronobiology Int.*, vol. 35, no. 10, pp. 1413–1422, Oct. 2018, doi: 10.1080/07420528.2018.1486852.

[8] P. Zontone, A. Affanni, R. Bernardini, A. Piras, and R. Rinaldo, "Low-complexity classification algorithm to identify drivers' stress using electrodermal activity (EDA) measurements," in *Proc. World Thematic Conf.-Biomed. Eng. Comput. Intell. (BIOCOM)*. Cham, Switzerland: Springer, Jul. 2019, pp. 25–33.

[9] S. Majumder, T. Mondal, and M. J. Deen, "Wearable sensors for remote health monitoring," *Sensors (Switzerland)*, vol. 17, no. 1, p. 130, Jan. 2017.

[10] F. Al Machot, A. Elmachot, M. Ali, E. Al Machot, and K. Kyamakya, "A deep-learning model for subject-independent human emotion recognition using electrodermal activity sensors," *Sensors*, vol. 19, no. 7, p. 1659, 2019. [Online]. Available: https://www.mdpi.com/1424-8220/19/7/1659

[11] S. Andersson, P. M. Gundersen, and A. Finset, "Emotional activation during therapeutic interaction in traumatic brain injury: Effect of apathy, self-awareness and implications for rehabilitation," *Brain Injury*, vol. 13, no. 6, pp. 393–404, Jan. 1999, doi: 10.1080/026990599121458.

[12] H. F. Nweke, Y. W. Teh, G. Mujtaba, and M. A. Al-Garadi, "Data fusion and multiple classifier systems for human activity detection and health monitoring: Review and open research directions," *Inf. Fusion*, vol. 46, pp. 147–170, Mar. 2019.

[13] S. Li, B. Sung, Y. Lin, and O. Mitas, "Electrodermal activity measure: A methodological review," *Ann. Tourism Res.*, vol. 96, Sep. 2022, Art. no. 103460.

[14] M. Ragot, N. Martin, S. Em, N. Pallamin, and J.-M. Diverrez, "Emotion recognition using physiological signals: Laboratory vs. Wearable sensors," in *Advances in Intelligent Systems and Computing*, vol. Springer, 2018, pp. 15–22.

[15] A. Sano and R. W. Picard, "Stress recognition using wearable sensors and mobile phones," in *Proc. Humaine Assoc. Conf. Affect. Comput. Intell. Interact.*, Sep. 2013, pp. 671–676.

[16] J. A. Castro-García, A. J. Molina-Cantero, M. Merino-Monge, and I. M. Gómez-González, "An open-source hardware acquisition platform for physiological measurements," *IEEE Sensors J.*, vol. 19, no. 23, pp. 11526–11534, Aug. 2019.

[17] J. Buekers et al., "Wearable finger pulse oximefor continuous oxygen saturation measurements during daily home routines of patients with chronic obstructive pulmonary disease (COPD) over one week: Observational study," *JMIR mHealth uHealth*, vol. 7, no. 6, Jun. 2019, Art. no. e12866.

[18] J. O. Olmedo-Aguirre, J. Reyes-Campos, G. Alor-Hernández, I. Machorro-Cano, L. Rodríguez-Mazahua, and J. L. Sánchez-Cervantes, "Remote healthcare for elderly people using wearables: A review," *Biosensors*, vol. 12, no. 2, p. 73, Jan. 2022.

[19] Y. Wang et al., "Recent advancements in flexible and wearable sensors for biomedical and healthcare applications," *J. Phys. D, Appl. Phys.*, vol. 55, no. 13, Mar. 2022, Art. no. 134001.

[20] S. Patel, H. Park, P. Bonato, L. Chan, and M. Rodgers, "A review of wearable sensors and systems with application in rehabilitation," *J. Neuroeng. Rehabil.*, vol. 9, no. 1, p. 21, Dec. 2012. [Online]. Available: http://www.jneuroengrehab.com/content/9/1/21

[21] G. Giannakakis, D. Grigoriadis, K. Giannakaki, O. Simantiraki, A. Roniotis, and M. Tsiknakis, "Review on psychological stress detection using biosignals," *IEEE Trans. Affect. Comput.*, vol. 13, no. 1, pp. 440–460, Jan. 2022.

[22] T. Q. Trung and N.-E. Lee, "Flexible and stretchable physical sensor integrated platforms for wearable human-activity monitoring and personal healthcare," *Adv. Mater.*, vol. 28, no. 22, pp. 4338–4372, Jun. 2016.

[23] C. Wan, D. Chen, Z. Huang, and X. Luo, "A wearable head mounted display bio-signals pad system for emotion recognition," *Sensors*, vol. 22, no. 1, p. 142, Dec. 2021, doi: 10.3390/s22010142.

[24] H. Feng, H. M. Golshan, and M. H. Mahoor, "A wavelet-based approach to emotion classification using EDA signals," *Expert Syst. Appl.*, vol. 112, pp. 77–86, Dec. 2018.

[25] N. Ganapathy, Y. R. Veeranki, and R. Swaminathan, "Convolutional neural network based emotion classification using electrodermal activity signals and time-frequency features," *Expert Syst. Appl.*, vol. 159, Nov. 2020, Art. no. 113571.

[26] D. Yu and S. Sun, "A systematic exploration of deep neural networks for EDA-based emotion recognition," *Information*, vol. 11, no. 4, p. 212, Apr. 2020.

[27] K. iMotions, "Galvanic skin response: The complete pocket guide," *Sci. Teach*, 2017.

[28] M. van Dooren, J. J. G.-J. de Vries, and J. H. Janssen, "Emotional sweating across the body: Comparing 16 different skin conductance measurement locations," *Physiol. Behav.*, vol. 106, no. 2, pp. 298–304, May 2012.

[29] D. S. Bari, "Gender differences in tonic and phasic electrodermal activity components," *Sci. J. Univ. Zakho*, vol. 8, no. 1, pp. 29–33, Mar. 2020.

[30] D. Jaiswal et al., "Assessment of cognitive load from biopotentials measured using wearable endosomatic device," in *Proc. 6th ACM Workshop Wearable Syst. Appl.*, Jun. 2020, pp. 13–18.

[31] W. Boucsein et al., "Publication recommendations for electrodermal measurements," *Psychophysiology*, vol. 49, no. 8, pp. 1017–1034, Aug. 2012.

[32] A. E. de Normalización. (2022). *Equipos Electromédicos. Parte 1: Requisitos Generales Para La Seguridad Básica Y Funcionamiento Esencial*. AENOR. [Online]. Available: https://tienda.aenor.com/norma-une-en-60601-1-2008-a13-2024-n0072893

[33] O. Pabst, C. Tronstad, S. Grimnes, D. Fowles, and Ø. G. Martinsen, "Comparison between the AC and DC measurement of electrodermal activity," *Psychophysiology*, vol. 54, no. 3, pp. 374–385, Mar. 2017.

[34] H. F. Posada-Quintero and K. H. Chon, "Innovations in electrodermal activity data collection and signal processing: A systematic review," *Sensors*, vol. 20, no. 2, p. 479, Jan. 2020.

[35] J. Wu et al., "Design of a portable electrochemical impedance spectroscopy measurement system based on AD5941 for lithium-ion batteries," *J. Energy Storage*, vol. 84, Apr. 2024, Art. no. 110856. [Online]. Available: https://www.sciencedirect.com/science/article/pii/S2352152X24004407

[36] N. Tran, N. Ha-Phan, T. Phan, C. T. S. Ching, and M. Ha, "Design and implementation of a cost-effective, portable impedance analyzer device with AD5941," *IEEJ Trans. Electr. Electron. Eng.*, vol. 19, no. 10, pp. 1730–1736, Oct. 2024. [Online]. Available: https://onlinelibrary.wiley.com/doi/abs/10.1002/tee.24134

[37] C. T. Nhu et al., "Research and development of a portable impedance measurement system utilizing AD5941 analog integrated circuit for A549 lung cancer cell detection," in *Proc. 1st Int. Conf. Health Sci. Technol. (ICHST)*, Dec. 2023, pp. 1–6.

[38] R. Song and M. Zhang, "Design and performance evaluation of an in situ online soil electrical conductivity sensor prototype based on the high-performance integrated chip AD5941," *Appl. Sci.*, vol. 14, no. 17, p. 7788, Sep. 2024.

[39] M. R. Baidillah et al., "Electrical impedance spectroscopy for skin layer assessment: A scoping review of electrode design, measurement methods, and post-processing techniques," *Measurement*, vol. 226, Feb. 2024, Art. no. 114111. [Online]. Available: https://www.sciencedirect.com/science/article/pii/S0263224123016755

[40] D. Asiain, J. Ponce de León, and J. R. Beltrán, "MsWH: A multisensory hardware platform for capturing and analyzing physiological emotional signals," *Sensors*, vol. 22, no. 15, p. 5775, Aug. 2022. [Online]. Available: https://www.mdpi.com/1424-8220/22/15/5775

[41] C. Chacha, D. Asiain, J. P. de León, and J. R. Beltrán, "Electrodermal activity measurement using constant current AC source," *Int. J. Biomed. Biol. Eng.*, vol. 18, no. 7, pp. 41–46, 2024. [Online]. Available: https://publications.waset.org/vol/211

[42] M. Saleh, S. Medina-Lombardero, M. L. Crichton, and A. J. Casson, "A portable electrical impedance measurement system for flexible electrodes," in *Proc. IEEE SENSORS*, Oct. 2024, pp. 1–4.

[43] M. F. Canabal, J. A. Miranda, J. M. Lanza-Gutiérrez, A. I. P. Garcilópez, and C. López-Ongil, "Electrodermal activity smart sensor integration in a wearable affective computing system," in *Proc. 35th Conf. Design Circuits Integr. Syst. (DCIS)*, Nov. 2020, pp. 1–6.

David Asiain Ansorena received B.Sc. degree in electronic engineering from the University of Zaragoza, Spain, in 2009, and the Ph.D. degrees in electronic engineering from Alfonso X el Sabio, Toledo, Spain, in 2017.

He is currently an Associate Professor of electronics with the Escuela Politécnica de la Almunia, University of Zaragoza, and a Member of the Research Group on Advanced Interfaces (AffectiveLab), Aragon Institute of Engineering Research, University of Zaragoza. His current research interests include wearable sensors, wireless sensor networks, the Internet of Things, MEMS inertial measurement units, and intelligent instrumentation.

Jesús Ponce de León Vázquez received the B.Sc. and Ph.D. degrees in physics from the University of Zaragoza, Zaragoza, Spain, in 1997 and 2012, respectively.

He is currently an Associate Professor of electronics with the Polytechnic School of la Almunia, University of Zaragoza, and a Member of the Research Group on Advanced Interfaces (AffectiveLab), Aragon Institute of Engineering Research, University of Zaragoza. His current research interests include wearable sensors and the processing and analysis of signals.

José Ramón Beltrán Blázquez received the B.Sc. and Ph.D. degrees in physics from the University of Zaragoza, Zaragoza, Spain, in 1988 and 1994, respectively.

He is currently an Associate Professor with the Department of Electronic Engineering and Communications, University of Zaragoza. In 2008, he was a Promoter and the Founder of an academic spin-off ARSTIC Audiovisual Solutions S.L., Zaragoza, which is devoted to the use of technologies for the artistic and audiovisual fields. He is a Member of the Research Group in Advanced Interfaces (AffectiveLab), Aragón Institute for Engineering Research, University of Zaragoza. He is involved in different research and development projects on audio analysis and processing. His research interests include automatic learning systems for the analysis, processing, and synthesis of musical signals.